Published in final edited form as:
Neurobiol Dis. 2014 July ; 67: 1–8. doi:10.1016/j.nbd.2014.02.007.

Diffusion fMRI detects white-matter dysfunction in mice with acute optic neuritis

Tsen-Hsuan Lin[1,*], **William M. Spees**[2,5], **Chia-Wen Chiang**[2], **Kathryn Trinkaus**[3], **Anne H. Cross**[4,5], and **Sheng-Kwei Song**[2,5]

[1]Department of Physics, Washington University, St. Louis, MO 63130, USA

[2]Department of Radiology, Washington University School of Medicine, St. Louis, MO 63110, USA

[3]Department of Biostatistics, Washington University School of Medicine, St. Louis, MO 63110, USA

[4]Department of Neurology, Washington University School of Medicine, St. Louis, MO 63110, USA

[5]Hope Center for Neurological Disorders, Washington University School of Medicine, St. Louis, MO 63110, USA

Abstract

Optic neuritis is a frequent and early symptom of multiple sclerosis (MS). Conventional magnetic resonance (MR) techniques provide means to assess multiple MS-related pathologies, including axonal injury, demyelination, and inflammation. A method to directly and non-invasively probe white-matter function could further elucidate the interplay of underlying pathologies and functional impairments. Previously, we demonstrated a significant 27% activation-associated decrease in the apparent diffusion coefficient of water perpendicular to the axonal fibers ($ADC_{\perp}$) in normal C57BL/6 mouse optic nerve with visual stimulation using diffusion fMRI. Here we apply this approach to explore the relationship between visual acuity, optic nerve pathology, and diffusion fMRI in the experimental autoimmune encephalomyelitis (EAE) mouse model of optic neuritis. Visual stimulation produced a significant 25% (vs. baseline) $ADC_{\perp}$ decrease in sham EAE optic nerves, while only a 7% (vs. baseline) $ADC_{\perp}$ decrease was seen in EAE mice with acute optic neuritis. The reduced activation-associated $ADC_{\perp}$ response correlated with post-MRI immunohistochemistry determined pathologies (including inflammation, demyelination, and axonal injury). The negative correlation between activation-associated $ADC_{\perp}$ response and visual acuity was also found when pooling EAE-affected and sham groups under our experimental criteria. Results suggest that reduction in diffusion fMRI directly reflects impaired axonal-

Corresponding Author: Sheng-Kwei "Victor" Song, Ph.D., Biomedical MR Laboratory, Campus Box 8227, Washington University School of Medicine, Room 2313, 4525 Scott Ave, St Louis, MO 63110, USA, Fax: +1 314 362 0526, Phone: +1 314 362 9988, ssong@wustl.edu.
*Current Address: Institute of Biomedical Sciences, Academia Sinica, Taipei City 11529, Taiwan (R.O.C.)

activation in EAE mice with optic neuritis. Diffusion fMRI holds promise for directly gauging *in vivo* white-matter dysfunction or therapeutic responses in MS patients.

Keywords

diffusion fMRI; white matter; EAE; optic neuritis; visual acuity

Introduction

Multiple sclerosis (MS) is an inflammatory demyelinating disease affecting brain, optic nerve, and spinal cord (Compston and Coles, 2008; Filippi et al., 2012; Trapp and Nave, 2008). Optic neuritis is a frequent first sign of MS, which produces blurred vision and/or pain in the affected eye due to inflammation and demyelination at foci within optic nerve (Arnold, 2005; Beck et al., 2003; Brodsky et al., 2008). Experimental autoimmune encephalomyelitis (EAE) induced by inoculation of myelin oligodendrocyte glycoprotein (MOG) peptide is a widely used animal model of human MS. Many features of the pathology in this EAE model resemble those characteristic of MS, including inflammation, demyelination, and axonal injury and loss (Diem et al., 2008; Emerson et al., 2009; Gold et al., 2006; Sun et al., 2007).

Magnetic resonance imaging (MRI) is routinely used to detect and quantify pathologies in EAE animal models and MS patients (Emerson et al., 2009; Filippi, 2003; Filippi et al., 2012; Ge, 2006; Inglese and Bester, 2010). For instance, diffusion-MRI-derived axial diffusivity, radial diffusivity, fractional anisotropy, and mean diffusivity have been used to identify axonal injury, demyelination, inflammation, and axonal loss (Naismith et al., 2010; Roosendaal et al., 2009; Song et al., 2005; Sun et al., 2007; Wu et al., 2007). Abnormal T2-weighted hyperintensities within white matter may reflect several pathologies, including inflammation, demyelination, and axonal loss (Bruck et al., 1997; Sahraian and Eshaghi, 2010). Significant axon loss can lead to persistent T1-weighted hypointensities (van Walderveen et al., 1998). T1-weighted gadolinium contrast-enhancement is indicative of compromised blood-brain barrier (BBB), which is associated with inflammation in EAE models and MS (Boretius et al., 2008; Broom et al., 2005; Bruck et al., 1997; Filippi et al., 1995; Nessler et al., 2007). More accurate and novel approaches have recently been introduced to distinguish coexisting inflammation, demyelination, and axonal injury using diffusion basis spectrum image (DBSI) or diffusion kurtosis image (DKI) (Chiang et al., 2012; Raz et al., 2013; Tu et al., 2012; Wang et al., 2011).

MRI also holds potential to probe functional integrity in real time. For instance, blood oxygen level dependent (BOLD) fMRI has been applied to study brain plasticity and cortical activation in MS patients (Gallo et al., 2012; Rocca et al., 2012a; Rocca et al., 2012b; Staffen et al., 2002) as a reflection of motor or visual functional deficits. However, conventional BOLD fMRI relies on local modulation of blood volume and blood flow, secondary to neuronal activation and metabolic demand, it is an approach which is largely limited to cortical and gray-matter regions (Heeger and Ress, 2002; Logothetis, 2008) and mainly reflects post-synaptic activity in cortical regions (Gawryluk et al., 2009; Logothetis

et al., 2001). Since EAE and MS are diseases that significantly affect white-matter tracts, a method to directly assess white-matter function (in combination with BOLD fMRI in gray matter) could provide more comprehensive information about disease progression and therapeutic response in experimental models and the clinic.

Diffusion fMRI has recently been introduced and suggested as an alternative approach to directly identify functional integrity of neurons and axons (Darquie et al., 2001; Flint et al., 2009; Le Bihan, 2012; Le Bihan et al., 2006; Spees et al., 2013; Tsurugizawa et al., 2013). Diffusion fMRI offers a promising means to assess axonal function since BOLD-based fMRI has not been successful in white matter and our previous report showed a significant 27% $ADC_{\perp}$ decrease during visual stimulation in healthy mouse optic nerves. Importantly, this activation-associated $ADC_{\perp}$ decrease in optic nerves was found to be independent of any vascular contribution (Spees et al., 2013).

In the current study, diffusion fMRI was evaluated as a non-invasive probe of *in vivo* optic nerve axonal dysfunction in mice with acute-stage EAE with unilateral optic neuritis. The prevalence of optic neuritis in the disease course of MS provides motivation for the current studies. Moreover, the optic nerve can be viewed as a prototypical white-matter structure, thus the current investigation lays the groundwork for future studies of MS pathophysiology and therapeutic outcome in other CNS white-matter targets.

Materials and Methods

All experimental procedures involving animals were approved by Washington University's Animal Studies Committee and conformed to the NIH Policy on Responsibility for Care and Use of Animals.

Experimental autoimmune encephalomyelitis (EAE) mouse model

Fourteen 7-week-old, female C57BL/6 mice were obtained from Jackson Laboratory (Bar Harbor, ME). Before immunization, mice were housed under a 12-hour dark/light cycle for a week. Mice were randomly separated into two groups: seven in the EAE group and seven in the sham group. The mice in the EAE group were immunized with 50 μg MOG_{35-55} peptide emulsified (1:1) in incomplete Freund's adjuvant (IFA) and desiccated Mycobacterium tuberculosis. Pertussis toxin (300 ng; PTX, List Laboratories, Campbell, CA) was injected intravenously on the day of MOG_{35-55} immunization and two days later. Mice in the sham control group underwent the same procedure with only IFA and pertussis toxin injected.

Visual Acuity (VA)

Mouse visual acuity was assessed using the Virtual Optometry System (OptoMotry, CerebralMechanics, Inc., Canada). Briefly, virtual rotating columns (vertical light/dark bands) were projected onto four LCD monitors, surrounding a platform where the mouse stands, with varied spatial frequencies in cycles/degree (c/d). The mouse head movement in response to the virtual column rotations was noted. The spatial frequency was changed starting from 0.1 c/d in increments or decrement of 0.05 c/d until the mouse stopped responding. The VA was defined as the highest spatial frequency of virtual rotating columns to which the mouse responded. Before immunization, normal VA was confirmed for each

eye (n = 28, VA = 0.37 ± 0.02 c/d) to exclude mice with poor vision at baseline due to unrelated factors. After immunization, VA was assessed daily in all mice. For animals in the EAE group, VA ≤ 0.25 c/d (8 – 13 days post-immunization) was defined as the onset of acute optic neuritis (Chiang et al., 2012). For EAE animals, diffusion fMRI measurements were performed on the first day (10.6 ± 1.7 days post-immunization, mean ± SD) at which their VA was observed to be below 0.25 c/d, at which time the VA decline was invariably unilateral. The mice in the sham group did not develop visual impairment, but underwent the diffusion fMRI procedure within the same time range (10.6 ± 1.7 days post-immunization, mean ± SD).

Animal anesthesia and set-up

For initial setup, mice were anesthetized with 1.5% isofluorane in O_2. Anesthetized mice were placed in a custom-made stereotactic head holder. The experimental eye remained open to receive light stimulus. The contralateral eye was covered with Parafilm™ and two layers of black electrical tape to block out the flashing light (also identified as “blocked” eyes in the text). After careful setup the mouse and head holder were placed in the imaging cradle. Respiratory rate and body temperature were monitored during experiments using an MR-compatible animal-monitoring system (SA Instrument, Inc., Stony Brook, NY). The body temperature was maintained at 37 °C via a regulated circulating warm water pad underneath the mouse body and regulated warm air blown into the magnet bore. When mouse respiration was stable, a subcutaneous 0.3 mg/kg bolus of medetomidine was administered followed immediately by a continuous infusion of medetomidine at a rate of 0.6 mg/kg·hr through an in-dwelling subcutaneous catheter. Isoflurane in the breathing-gas mixture was gradually discontinued according to previously-described protocols until the animals were breathing room air (Adamczak et al., 2010).

Diffusion-weighted Image (DWI) protocol

MRI experiments were performed on a 4.7-T Agilent DirectDrive™ small-animal MRI system (Agilent Technologies, Santa Clara, CA) equipped with a Magnex/Agilent HD imaging gradient coil (Magnex/Agilent, Oxford, UK) capable of pulsed-gradient strengths of up to 58 G/cm and a gradient rise time ≤ 295 μs. An actively-decoupled 1.7-cm receive-only surface coil was positioned on top of the mouse head. Then, the animal holder assembly, including the receive coil was placed inside an 8-cm actively-decoupled volume transmit coil.

DWI measurements were carried out as previously described (Spees et al., 2013). In brief, a multi-echo spin-echo diffusion-weighted imaging sequence (Tu et al., 2010) was employed to improve the signal-to-noise ratio (SNR) by averaging the extra echoes of the same k-space line, during the readout period after diffusion weighting, with negligible increase in imaging time comparing with the conventional spin-echo diffusion sequence. A train of three echoes were co-added to increase signal-to-noise in the summed MR image. The following acquisition parameters were used: TR = 1.5 s, TE = 37.1 ms, inter-echo delay = 23.6 ms, FOV = 20 × 20 mm^2, matrix size = 256 × 256 (zero-filled to 512 × 512), slice thickness = 1.3 mm. To obtain the final target image plane and minimize partial volume effects, a middle-sagittal DW image (diffusion gradient applied in the slice-select direction)

was acquired based on axial scout images. The sagittal DWI encompassed optic nerves of both eyes longitudinally. An image plane parallel to the optic nerves was placed overlying the nerves. By rotating this image plane by 90°, the final targeted image slice plane was orthogonal to the optic nerves to minimize partial volume effects. Two diffusion-sensitizing factors (b values), 0.1 and 1.4 ms/μm^2, i.e., 100 and 1400 s/mm^2 (with δ = 5 ms and Δ = 18 ms), were applied to generate a pair of DWIs (Fig. 1 A and B).

Visual stimulation

Visual stimulation was delivered by a flashing white LED (Cree, Model C503C-WAS) placed 5 cm in front of the mouse nose, the corresponding luminance level ~ 445 candela/m^2. A step-function signal of 4V amplitude was repeated at 1.4 Hz with 200/514 ms on/off duration to generate the flashing light stimulus. Equipment set-up was as reported previously (Spees et al., 2013).

Diffusion fMRI strategy

For each mouse, three pairs of diffusion-weighted images were acquired. The first pair of images without visual stimulation was taken as a baseline. Then, the stimulus-on DWI dataset was acquired during application of flashing-light stimulation. Finally, the LED light was turned off for the post-stimulus DWI acquisition.

DWI Data analysis

For measurements of diffusion perpendicular to the axonal fibers, signal decay with b-value between 0.1 and 1.4 ms/μm^2 (or 100 and 1400 s/mm^2) is mono-exponential (Spees et al., 2013). $ADC_{\perp}$ maps were generated from the pair of DWIs according to the Skejskal-Tanner equation (Stejskal and Tanner, 1965) with code developed in-house and written in MATLAB (Mathworks, Natick, MA). Optic nerve ROIs were drawn based on operator-independent criteria as described previously (Spees et al., 2013).

Immunohistochemistry (IHC) staining in optic nerves

Following MR experiments, mice were perfused with 0.01 M phosphate-buffered saline (PBS) followed by 4% paraformaldehyde in 0.01 M PBS. The brain was excised and post-fixed in 4% paraformaldehyde/PBS for 24 hours then transferred to 0.01 M PBS for storage at 4 °C until histological analysis. Mouse optic nerves were embedded in 2% agar blocks (Blewitt et al., 1982). Then, the agar block was embedded in paraffin wax and 5-μm thick transverse slices were sectioned for IHC staining. Sections were deparaffinized, rehydrated, and then blocked using 1% bovine serum albumin (BSA, Sigma Inc., MO, US) and 5% normal goat-serum solution for 20 minutes at room temperature to prevent non-specific binding. Slides were incubated overnight at 4 °C with monoclonal anti-phosphorylated neurofilament antibody (SMI-31; 1:1000, Covance, U.S.) to stain non-injured axons or with rabbit anti-myelin basic protein (MBP) antibody (1:1000, Sigma Inc., MO, U.S.) to stain myelin sheaths (Budde et al., 2009; Song et al., 2003; Sun et al., 2008). After rinsing, goat anti-mouse IgG or goat anti-rabbit IgG conjugated Alexa 488 (1:800) were applied to visualize immunoreactivity of phosphorylated neurofilament and MBP. Finally, slides were covered using Vectashield Mounting Medium with 4′,6-diamidino-2-phenylindole (DAPI,

Vector Laboratory, Inc., Burlingame, CA) to stain cell nuclei (Budde et al., 2009; Wang et al., 2011). Histological slides were examined with a Nikon Eclipse 80i fluorescence microscope equipped with a 60× water objective, and images from the center of optic nerve were captured with a black-and-white CCD camera with MetaMorph software (Universal Imaging Corporation, Sunnyvale, CA). The 60× IHC images (0.018 mm^2) covered ~40% of the whole optic nerve area (0.045 ± 0.013 mm^2, mean ± SD). Histological counts are reported for 7 EAE-affected and 6 sham optic nerves in this study (one sham optic nerve specimen was damaged during tissue processing).

Histological data analysis

Whole-field SMI-31, MBP, and DAPI images at 60× magnification were captured with the same fluorescence light intensity and exposure time. All captured images were converted to 8-bit gray scale and analyzed using threshold, particle analyzer and gray level watershed segmentation functions in ImageJ (http://bigwww.epfl.ch/sage/soft/watershed/).

Statistical analysis

$ADC_{\perp}$ changes (initial/baseline vs. stimulus on, stimulus on vs. stimulus off, etc.) were tested for statistical significance via a cluster linear repeated measures model, which took into account that there were three time points for each eye and two eyes per mouse. The p-values of visual function (VA), SMI-31, MBP, and DAPI were from nonparametric Wilcoxon two-sample tests for difference between sham and EAE groups. The correlation coefficients for VA with each of SMI-31, MBP, DAPI, and decreased $ADC_{\perp}$ were analyzed by Spearman's rank correlation coefficient.

Results

Impairment of visual function and reduced activation-associated $ADC_{\perp}$ response in EAE optic nerves

For animals in the EAE group, the onset of optic neuritis, defined as VA ≤ 0.25 c/d (Chiang et al., 2012), occurred in the range from 8 – 13 days post-immunization (10.6 ± 1.7 days post-immunization, mean ± SD). Group-averaged visual acuities of the EAE-affected (optic neuritis), sham and blocked eyes (n= 7, 7, and 14, respectively) were 0.15 ± 0.08, 0.36 ± 0.02, and 0.36 ± 0.03 c/d (mean ± SD, Fig. 2 A). Since all EAE-affected mice in this study developed unilateral visual impairment, the VA of blocked eyes (n = 14) were in the normal range. VA of EAE-affected eyes with optic neuritis showed a significant 58% decrease ($p < 0.005$, EAE vs. sham) in measurements just prior to diffusion fMRI.

$ADC_{\perp}$ maps were generated from the diffusion-weighted image data (Fig. 1). The group-averaged baseline optic-nerve $ADC_{\perp}$ of affected acute-stage EAE optic neuritis eyes was higher than in sham eyes (Fig. 2 B and 2 C, Table 1). Compared to their own pre-stimulus baseline and stimulus off measurements, $ADC_{\perp}$ during visual stimulus of EAE-affected versus sham eyes showed no significant (7%, $p = 0.45$, vs. baseline and 10%, $p = 0.15$, vs. stimulus off for EAE) versus significant (25%, $p < 0.005$, vs. baseline and 22 %, $p < 0.005$, vs. stimulus off for sham) decrease, respectively. No $ADC_{\perp}$ changes were observed between baseline, stimulus on, and stimulus off in the contralateral blocked eyes of mice with EAE (p

= 0.91 for baseline vs. stimulus on and p = 0.13 for stimulus on vs. stimulus off) and sham (p = 0.97 for baseline vs. stimulus on and p = 0.64 for stimulus on vs. stimulus off) mice (Fig. 2 B and C, Table 1). Thus EAE-affected eyes with optic neuritis as evinced by impaired visual acuity exhibited a correspondingly reduced $ADC_{\perp}$ response with visual stimulation.

Axonal impairment was assessed by immunohistochemistry (IHC) staining

Previously, we have employed immunohistochemical (IHC) staining of phosphorylated neurofilaments (SMI-31, intact axons), myelin basic protein (MBP, myelin sheath), and 4′, 6- diamidino-2-phenylindole (DAPI, cell nuclei) to reflect white-matter integrity (Song et al., 2003; Sun et al., 2007; Wang et al., 2011). Representative zoomed-in 60× images (56% of the 60× field of view) from EAE-affected (n=7) optic nerves demonstrated axonal beading, with lower density of intact axons, less myelin positive area (with thinner myelin), and higher density of cell nuclei (Fig. 3A, D, and G) than sham optic nerves (n = 6). Group-averaged analysis of SMI-31, MBP, and DAPI (Fig. 3C, F, I and Table 2) at EAE optic neuritis onset showed a significant 22% decrease in density of intact axons [$p < 0.005$, 5.3 (± 0.6) × 10^5 mm^{-2}] and 17% decrease in myelin sheath area [$p < 0.005$, 36.2 (± 2.5) %] compared with sham group [6.8 (± 0.5) × 10^5 mm^{-2} and 43.6 (± 2.1) %, respectively]. Furthermore, the density of cell nuclei in optic nerves at EAE optic neuritis onset was increased by 38% [$p < 0.05$, 5.8 (± 1.2) × 10^3 mm^{-2}] compared with sham group [4.2 (± 0.5) × 10^3 mm^{-2}]. Based on IHC results, the EAE-affected optic nerves demonstrated unequivocal signs of axonal injury, demyelination, and inflammation.

Reduced activation-associated $ADC_{\perp}$ was correlated with impaired visual function and optic nerve pathologies

The correlation between activation-associated $ADC_{\perp}$ response and visual acuity was found when pooling EAE and sham groups under our experimental criteria (Fig. 4A, r = 0.76, p = 0.0015), axon density (Fig. 4B, r = 0.92, $p < 0.0001$), and myelin sheath area (Fig. 4C, r = 0.76, p = 0.0023) and, to a lesser degree, with cell nuclei density (Fig. 4D, r = 0.60, p = 0.03). The data suggest that diffusion fMRI can provide a means to non-invasively and directly assess axonal dysfunction associated with axonal injury, demyelination, and inflammation at optic neuritis onset in this EAE mouse model.

Discussion

This is the first study applying diffusion fMRI to assess functional deficits of a white-matter tract *in vivo*. The results presented here demonstrate an attenuated neuronal-activation-associated $ADC_{\perp}$ response (~7% non-significant reduction) in EAE mice at the onset of optic neuritis, compared to a significant decremental response in sham mice (~25% reduction). The results for EAE sham mice are comparable to our previously-reported ~27% $ADC_{\perp}$ decrease in optic nerves of normal mice (Spees et al., 2013). Reduced activation-associated $ADC_{\perp}$ response in association with impaired visual function (Fig. 4A) correlated with underlying optic-nerve axonal pathology (Fig. 3).

Visual signal conduction through the optic nerve depends on repeated cycles of membrane depolarization/action potential/repolarization, which are accompanied by ion gradient changes (Nicholls et al., 2001; Zhang et al., 2006). Unlike BOLD fMRI, which is largely limited to gray matter (Gawryluk et al., 2009; Logothetis et al., 2001), we proposed that diffusion fMRI could detect the effect of functional activation of axons and further improves our understanding of CNS functionality. Extracellular space (ECS) shrinkage during electrical stimulation has been reported (Holthoff and Witte, 1996; Nicholson and Sykova, 1998; Ransom and Orkand, 1996; Ransom et al., 1985), such ECS shrinkage is highly associated with transient ionic gradient changes, osmotic shifts of water across cell membranes, or glial cell swelling associated with changes in size and shape (Bay and Butt, 2012; Flint et al., 2009; Kole et al., 2008; Le Bihan, 2007; Le Bihan and Johansen-Berg, 2012; Schwartzkroin et al., 1998; Waxman, 1977). We speculated that diffusion measurement, especially, in white matter would be sensitive to extracellular space (ECS) shrinkage with relative minor vascular-coupling effect due to lower blood flow and volume. Therefore, the activation-associated $ADC_{\perp}$ decrease of diffusion fMRI is expected. Indeed, in our previous study, an activation-associated 27% $ADC_{\perp}$ decrease in healthy mouse optic nerves was shown and observed to be independent of vascular-coupling contributions (Spees et al., 2013). In the same study, we did not observed $ADC_{\parallel}$ changes during the visual stimulation. We speculate that this may be due to that $ADC_{\parallel}$ is likely to be affected more by the intra-axonal water than that in the ECS. Hence, diffusion fMRI measuring $ADC_{\perp}$ of axonal bundles has the potential to directly probe axon functional integrity without confounding blood-flow effects.

For MS and its animal model, EAE, mitochondrial impairment reduces energy production due to increased nitric oxide and free radical/reactive oxygen species (Smith and Lassmann, 2002). Sodium channel redistribution in demyelinated axons is required to maintain signal propagation but this also increases energy consumption (Kornek et al., 2001; Waxman, 2006). The imbalanced energy cycle would eventually lead to energy deficiency associated Na^+/K^+-ATPase pump failure and the reversal of Na^+/Ca^{2+} exchanger due to increased intracellular Na^+. Finally, the resultant influx and accumulation of intracellular Ca^{2+} may further lead to mitochondrial dysfunction and axonal damage (Craner et al., 2005; Stys, 2005; Su et al., 2009). Optic neuritis is frequently the first sign of MS in patients (Beck et al., 2003). Inflammation and demyelination of the affected optic nerves are associated with impeded action potential conduction (Compston and Coles, 2008) and result in impaired visual function. In EAE animal models of MS, several reports demonstrated visual dysfunction accompanying optic neuritis via behavioral or visual evoked potential (VEP) measurements (Diem et al., 2008; Diem et al., 2005; Matsunaga et al., 2012; Meyer et al., 2001). These measurements rely upon functionality of the entire visual pathway including retina, optic nerve, visual cortex, and/or conscious response of the brain. Thus, they may lack specificity in the location and contribution of specific optic nerve/white-matter lesion sites. Ion-channel dysfunction and deregulation are related to impaired signal propagation. Ion-channel dysfunction and deregulation could also lead to disability of activation-associated modulation in ECS. Therefore, activation-associated $ADC_{\perp}$ decrease, which likely results from ECS shrinkage during axonal activation, was less in EAE-affected optic nerves than in sham mice optic nerves during visual stimulation.

In this study, visual acuity measurements in EAE and sham eyes represent overall function of the entire visual efferent pathway (Douglas et al., 2005; Prusky et al., 2004). If we accept that the VA measurement reflects overall electrophysiological competence as measured by VEP (Ridder and Nusinowitz, 2006), and that the optic nerve is the primary site of impaired visual function in this EAE animal model, then the VA measurement provides an indirect measure of optic nerve electrical competence. As expected, the VA of EAE optic neuritis eyes was significantly lower than in sham eyes (Fig. 2A) in the current study. Subsequent histological results of these same optic nerves revealed axonal injury, demyelination, and inflammation (Fig. 3C, F, and I), suggesting that these optic-nerve-specific pathologies were a primary source of the impaired visual function in EAE mice.

Based on VEP measurement in the mouse visual system, the optimal visual stimulation condition in C57BL/6 mice has been determined (Ridder and Nusinowitz, 2006) and applied to this study. During diffusion measurement with visual stimulation, decreased $ADC_{\perp}$ and unchanged $ADC_{\perp}$ were observed in unblocked and blocked normal (sham) eyes, respectively (Fig. 2B and C), suggesting the $ADC_{\perp}$ directly revealed the effect of functional activation in optic nerves. For the unblocked eyes, the $ADC_{\perp}$ change in EAE-affected optic nerves was less than sham optic nerves and provides some measure of the extent of axonal dysfunction (Fig. 2B and C).

Since contributions from retinal dysfunction at the early time point measured herein may (Quinn et al., 2011; Shindler et al., 2008) or may not (Meyer et al., 2001) be ruled out, the RGC (retinal ganglion cell) histological data of our own EAE model were confirmed before this study. The RGC counting results of sham and EAE-affected groups at these early time-points were no different, and suggested that RGC pathologies may occur later in the progression of optic neuritis (Chiang et al., unpublished). Therefore, the attenuated diffusion fMRI response (reduced $ADC_{\perp}$ decrease with stimulation) is likely a direct result of axonal dysfunction. The somewhat elevated baseline $ADC_{\perp}$ in EAE optic neuritis (Table 2) may result from acute demyelination or vasogenic edema since radial diffusivity or ADC increases reflecting those two pathologies have been reported in EAE mice and MS patients (Boretius et al., 2008; Castriota-Scanderbeg et al., 2002; Chiang et al., 2012; Hickman et al., 2004; Song et al., 2005; Sun et al., 2007).

Our results showed that the functional deficits in EAE-affected optic nerves using diffusion fMRI provide a unique perspective on the consequences of inflammatory demyelinating pathologies. Since the EAE optic neuritis nerves at the acute stage exhibit multiple coexisting pathologies, it is not possible to determine contributions of each specific type of tissue damage to the overall reduced activation-associated $ADC_{\perp}$ response. Consequently, pre-onset study for EAE optic neuritis would be needed to understand if functional deficits precede morphological changes and the inter-relationship between mild injury and diffusion fMRI activation. *In vivo* diffusion fMRI is a promising tool for direct investigations of evolving pathology, therapeutic targets, and/or longitudinal assessment in white-matter tracts.

Acknowledgments

The authors thank Mr. Bob Mikesell for excellent technical assistance. This study was supported in part by the grants from National Institute of Health R01-NS047592 (S.-K.S.), P01-NS059560 (A.H.C.), and National Multiple Sclerosis Society (NMSS) RG 4549A4/1 (S.-K.S.) and an NMSS Pilot Award PP1865 (W.M.S).

References

Adamczak JM, Farr TD, Seehafer JU, Kalthoff D, Hoehn M. High field BOLD response to forepaw stimulation in the mouse. Neuroimage. 2010; 51:704–712. [PubMed: 20211267]

Arnold AC. Evolving management of optic neuritis and multiple sclerosis. Am J Ophthalmol. 2005; 139:1101–1108. [PubMed: 15953446]

Bay V, Butt AM. Relationship between glial potassium regulation and axon excitability: a role for glial Kir4.1 channels. Glia. 2012; 60:651–660. [PubMed: 22290828]

Beck RW, Trobe JD, Moke PS, Gal RL, Xing D, Bhatti MT, Brodsky MC, Buckley EG, Chrousos GA, Corbett J, Eggenberger E, Goodwin JA, Katz B, Kaufman DI, Keltner JL, Kupersmith MJ, Miller NR, Nazarian S, Orengo-Nania S, Savino PJ, Shults WT, Smith CH, Wall M. High- and low-risk profiles for the development of multiple sclerosis within 10 years after optic neuritis: experience of the optic neuritis treatment trial. Arch Ophthalmol. 2003; 121:944–949. [PubMed: 12860795]

Blewitt ES, Pogmore T, Talbot IC. Double embedding in agar/paraffin wax as an aid to orientation of mucosal biopsies. J Clin Pathol. 1982; 35:365. [PubMed: 7068930]

Boretius S, Gadjanski I, Demmer I, Bahr M, Diem R, Michaelis T, Frahm J. MRI of optic neuritis in a rat model. Neuroimage. 2008; 41:323–334. [PubMed: 18394926]

Brodsky M, Nazarian S, Orengo-Nania S, Hutton GJ, Buckley EG, Massey EW, Bhatti MT, Greer M, Goodwin J, Wall M, Savino PJ, Leist T, Miller NR, Irani D, Trobe JD, Cornblath W, Kaufman DI, Eggenberger E, Kupersmith MJ, Shults WT, McAllister L, Hamilton S, Beck RW, Dontchev M, Gal RL, Kollman C, Keltner JL, Smith CH, Grp ONS. Multiple sclerosis risk after optic neuritis - Final optic neuritis treatment trial follow-up. Arch Neurol. 2008; 65:727–732. [PubMed: 18541792]

Broom KA, Anthony DC, Blamire AM, Waters S, Styles P, Perry VH, Sibson NR. MRI reveals that early changes in cerebral blood volume precede blood-brain barrier breakdown and overt pathology in MS-like lesions in rat brain. J Cereb Blood Flow Metab. 2005; 25:204–216. [PubMed: 15678123]

Bruck W, Bitsch A, Kolenda H, Bruck Y, Stiefel M, Lassmann H. Inflammatory central nervous system demyelination: correlation of magnetic resonance imaging findings with lesion pathology. Ann Neurol. 1997; 42:783–793. [PubMed: 9392578]

Budde MD, Xie M, Cross AH, Song SK. Axial diffusivity is the primary correlate of axonal injury in the experimental autoimmune encephalomyelitis spinal cord: a quantitative pixelwise analysis. J Neurosci. 2009; 29:2805–2813. [PubMed: 19261876]

Castriota-Scanderbeg A, Sabatini U, Fasano F, Floris R, Fraracci L, Mario MD, Nocentini U, Caltagirone C. Diffusion of water in large demyelinating lesions: a follow-up study. Neuroradiology. 2002; 44:764–767. [PubMed: 12221449]

Chiang CW, Wang Y, Lin TH, Cross AH, Song SK. Acute visual function impairment in EAE is primarily caused by optic nerve inflammation as assessed by DBSI. Proc Intl Soc Mag Reson Med. 2012; 20:3058.

Compston A, Coles A. Multiple sclerosis. Lancet. 2008; 372:1502–1517. [PubMed: 18970977]

Craner MJ, Damarjian TG, Liu S, Hains BC, Lo AC, Black JA, Newcombe J, Cuzner ML, Waxman SG. Sodium channels contribute to microglia/macrophage activation and function in EAE and MS. Glia. 2005; 49:220–229. [PubMed: 15390090]

Darquie A, Poline JB, Poupon C, Saint-Jalmes H, Le Bihan D. Transient decrease in water diffusion observed in human occipital cortex during visual stimulation. Proc Natl Acad Sci U S A. 2001; 98:9391–9395. [PubMed: 11459931]

Diem R, Demmer I, Boretius S, Merkler D, Schmelting B, Williams SK, Sattler MB, Bahr M, Michaelis T, Frahm J, Bruck W, Fuchs E. Autoimmune optic neuritis in the common marmoset monkey: comparison of visual evoked potentials with MRI and histopathology. Invest Ophthalmol Vis Sci. 2008; 49:3707–3714. [PubMed: 18450589]

Diem R, Sattler MB, Merkler D, Demmer I, Maier K, Stadelmann C, Ehrenreich H, Bahr M. Combined therapy with methylprednisolone and erythropoietin in a model of multiple sclerosis. Brain. 2005; 128:375–385. [PubMed: 15601662]

Douglas RM, Alam NM, Silver BD, McGill TJ, Tschetter WW, Prusky GT. Independent visual threshold measurements in the two eyes of freely moving rats and mice using a virtual-reality optokinetic system. Vis Neurosci. 2005; 22:677–684. [PubMed: 16332278]

Emerson MR, Gallagher RJ, Marquis JG, LeVine SM. Enhancing the ability of experimental autoimmune encephalomyelitis to serve as a more rigorous model of multiple sclerosis through refinement of the experimental design. Comp Med. 2009; 59:112–128. [PubMed: 19389303]

Filippi M. MRI-clinical correlations in the primary progressive course of MS: new insights into the disease pathophysiology from the application of magnetization transfer, diffusion tensor, and functional MRI. J Neurol Sci. 2003; 206:157–164. [PubMed: 12559504]

Filippi M, Campi A, Martinelli V, Colombo B, Yousry T, Canal N, Scotti G, Comi G. Comparison of triple dose versus standard dose gadolinium-DTPA for detection of MRI enhancing lesions in patients with primary progressive multiple sclerosis. J Neurol Neurosurg Psychiatry. 1995; 59:540–544. [PubMed: 8530944]

Filippi M, Rocca MA, Barkhof F, Bruck W, Chen JT, Comi G, DeLuca G, De Stefano N, Erickson BJ, Evangelou N, Fazekas F, Geurts JJ, Lucchinetti C, Miller DH, Pelletier D, Popescu BF, Lassmann H. Association between pathological and MRI findings in multiple sclerosis. Lancet Neurol. 2012; 11:349–360. [PubMed: 22441196]

Flint J, Hansen B, Vestergaard-Poulsen P, Blackband SJ. Diffusion weighted magnetic resonance imaging of neuronal activity in the hippocampal slice model. Neuroimage. 2009; 46:411–418. [PubMed: 19233299]

Gallo A, Esposito F, Sacco R, Docimo R, Bisecco A, Della Corte M, D'Ambrosio A, Corbo D, Rosa N, Lanza M, Cirillo S, Bonavita S, Tedeschi G. Visual resting-state network in relapsing-remitting MS with and without previous optic neuritis. Neurology. 2012; 79:1458–1465. [PubMed: 22972637]

Gawryluk JR, Brewer KD, Beyea SD, D'Arcy RC. Optimizing the detection of white matter fMRI using asymmetric spin echo spiral. Neuroimage. 2009; 45:83–88. [PubMed: 19084071]

Ge Y. Multiple sclerosis: the role of MR imaging. AJNR Am J Neuroradiol. 2006; 27:1165–1176. [PubMed: 16775258]

Gold R, Linington C, Lassmann H. Understanding pathogenesis and therapy of multiple sclerosis via animal models: 70 years of merits and culprits in experimental autoimmune encephalomyelitis research. Brain. 2006; 129:1953–1971. [PubMed: 16632554]

Heeger DJ, Ress D. What does fMRI tell us about neuronal activity? Nat Rev Neurosci. 2002; 3:142–151. [PubMed: 11836522]

Hickman SJ, Toosy AT, Jones SJ, Altmann DR, Miszkiel KA, MacManus DG, Barker GJ, Plant GT, Thompson AJ, Miller DH. A serial MRI study following optic nerve mean area in acute optic neuritis. Brain. 2004; 127:2498–2505. [PubMed: 15342363]

Holthoff K, Witte OW. Intrinsic optical signals in rat neocortical slices measured with near-infrared dark-field microscopy reveal changes in extracellular space. J Neurosci. 1996; 16:2740–2749. [PubMed: 8786449]

Inglese M, Bester M. Diffusion imaging in multiple sclerosis: research and clinical implications. NMR Biomed. 2010; 23:865–872. [PubMed: 20882528]

Kole MH, Ilschner SU, Kampa BM, Williams SR, Ruben PC, Stuart GJ. Action potential generation requires a high sodium channel density in the axon initial segment. Nat Neurosci. 2008; 11:178–186. [PubMed: 18204443]

Kornek B, Storch MK, Bauer J, Djamshidian A, Weissert R, Wallstroem E, Stefferl A, Zimprich F, Olsson T, Linington C, Schmidbauer M, Lassmann H. Distribution of a calcium channel subunit in dystrophic axons in multiple sclerosis and experimental autoimmune encephalomyelitis. Brain. 2001; 124:1114–1124. [PubMed: 11353727]

Le Bihan D. The 'wet mind': water and functional neuroimaging. Phys Med Biol. 2007; 52:R57–90. [PubMed: 17374909]

Le Bihan D. Diffusion, confusion and functional MRI. Neuroimage. 2012; 62:1131–1136. [PubMed: 21985905]

Le Bihan D, Johansen-Berg H. Diffusion MRI at 25: exploring brain tissue structure and function. Neuroimage. 2012; 61:324–341. [PubMed: 22120012]

Le Bihan D, Urayama S, Aso T, Hanakawa T, Fukuyama H. Direct and fast detection of neuronal activation in the human brain with diffusion MRI. Proc Natl Acad Sci U S A. 2006; 103:8263–8268. [PubMed: 16702549]

Logothetis NK. What we can do and what we cannot do with fMRI. Nature. 2008; 453:869–878. [PubMed: 18548064]

Logothetis NK, Pauls J, Augath M, Trinath T, Oeltermann A. Neurophysiological investigation of the basis of the fMRI signal. Nature. 2001; 412:150–157. [PubMed: 11449264]

Matsunaga Y, Kezuka T, An X, Fujita K, Matsuyama N, Matsuda R, Usui Y, Yamakawa N, Kuroda M, Goto H. Visual functional and histopathological correlation in experimental autoimmune optic neuritis. Invest Ophthalmol Vis Sci. 2012; 53:6964–6971. [PubMed: 22969072]

Meyer R, Weissert R, Diem R, Storch MK, de Graaf KL, Kramer B, Bahr M. Acute neuronal apoptosis in a rat model of multiple sclerosis. J Neurosci. 2001; 21:6214–6220. [PubMed: 11487644]

Naismith RT, Xu J, Tutlam NT, Trinkaus K, Cross AH, Song SK. Radial diffusivity in remote optic neuritis discriminates visual outcomes. Neurology. 2010; 74:1702–1710. [PubMed: 20498438]

Nessler S, Boretius S, Stadelmann C, Bittner A, Merkler D, Hartung HP, Michaelis T, Bruck W, Frahm J, Sommer N, Hemmer B. Early MRI changes in a mouse model of multiple sclerosis are predictive of severe inflammatory tissue damage. Brain. 2007; 130:2186–2198. [PubMed: 17617655]

Nicholls, JG.; Kuffler, SW.; Robert, MA. From neuron to brain. 4. Sinauer Associates; Sunderland, Mass: 2001.

Nicholson C, Sykova E. Extracellular space structure revealed by diffusion analysis. Trends Neurosci. 1998; 21:207–215. [PubMed: 9610885]

Prusky GT, Alam NM, Beekman S, Douglas RM. Rapid quantification of adult and developing mouse spatial vision using a virtual optomotor system. Invest Ophthalmol Vis Sci. 2004; 45:4611–4616. [PubMed: 15557474]

Quinn TA, Dutt M, Shindler KS. Optic neuritis and retinal ganglion cell loss in a chronic murine model of multiple sclerosis. Front Neurol. 2011; 2:50. [PubMed: 21852980]

Ransom BR, Orkand RK. Glial-neuronal interactions in non-synaptic areas of the brain: studies in the optic nerve. Trends Neurosci. 1996; 19:352–358. [PubMed: 8843605]

Ransom BR, Yamate CL, Connors BW. Activity-dependent shrinkage of extracellular space in rat optic nerve: a developmental study. J Neurosci. 1985; 5:532–535. [PubMed: 3973681]

Raz E, Bester M, Sigmund EE, Tabesh A, Babb JS, Jaggi H, Helpern J, Mitnick RJ, Inglese M. A Better Characterization of Spinal Cord Damage in Multiple Sclerosis: A Diffusional Kurtosis Imaging Study. AJNR Am J Neuroradiol. 2013

Ridder WH 3rd, Nusinowitz S. The visual evoked potential in the mouse--origins and response characteristics. Vision Res. 2006; 46:902–913. [PubMed: 16242750]

Rocca MA, Absinta M, Filippi M. The role of advanced magnetic resonance imaging techniques in primary progressive MS. J Neurol. 2012a; 259:611–621. [PubMed: 21814822]

Rocca MA, Valsasina P, Martinelli V, Misci P, Falini A, Comi G, Filippi M. Large-scale neuronal network dysfunction in relapsing-remitting multiple sclerosis. Neurology. 2012b; 79:1449–1457. [PubMed: 22955126]

Roosendaal SD, Geurts JJ, Vrenken H, Hulst HE, Cover KS, Castelijns JA, Pouwels PJ, Barkhof F. Regional DTI differences in multiple sclerosis patients. Neuroimage. 2009; 44:1397–1403. [PubMed: 19027076]

Sahraian MA, Eshaghi A. Role of MRI in diagnosis and treatment of multiple sclerosis. Clin Neurol Neurosurg. 2010; 112:609–615. [PubMed: 20417027]

Schwartzkroin PA, Baraban SC, Hochman DW. Osmolarity, ionic flux, and changes in brain excitability. Epilepsy Res. 1998; 32:275–285. [PubMed: 9761327]

Shindler KS, Ventura E, Dutt M, Rostami A. Inflammatory demyelination induces axonal injury and retinal ganglion cell apoptosis in experimental optic neuritis. Exp Eye Res. 2008; 87:208–213. [PubMed: 18653182]

Smith KJ, Lassmann H. The role of nitric oxide in multiple sclerosis. Lancet Neurol. 2002; 1:232–241. [PubMed: 12849456]

Song SK, Sun SW, Ju WK, Lin SJ, Cross AH, Neufeld AH. Diffusion tensor imaging detects and differentiates axon and myelin degeneration in mouse optic nerve after retinal ischemia. Neuroimage. 2003; 20:1714–1722. [PubMed: 14642481]

Song SK, Yoshino J, Le TQ, Lin SJ, Sun SW, Cross AH, Armstrong RC. Demyelination increases radial diffusivity in corpus callosum of mouse brain. Neuroimage. 2005; 26:132–140. [PubMed: 15862213]

Spees WM, Lin TH, Song SK. White-matter diffusion fMRI of mouse optic nerve. Neuroimage. 2013; 65:209–215. [PubMed: 23085108]

Staffen W, Mair A, Zauner H, Unterrainer J, Niederhofer H, Kutzelnigg A, Ritter S, Golaszewski S, Iglseder B, Ladurner G. Cognitive function and fMRI in patients with multiple sclerosis: evidence for compensatory cortical activation during an attention task. Brain. 2002; 125:1275–1282. [PubMed: 12023316]

Stejskal EO, Tanner JE. Spin Diffusion Measurements: Spin Echoes in the Presence of a Time-Dependent Field Gradient. The Journal of Chemical Physics. 1965; 42:288–292.

Stys PK. General mechanisms of axonal damage and its prevention. J Neurol Sci. 2005; 233:3–13. [PubMed: 15899499]

Su KG, Banker G, Bourdette D, Forte M. Axonal degeneration in multiple sclerosis: the mitochondrial hypothesis. Curr Neurol Neurosci Rep. 2009; 9:411–417. [PubMed: 19664372]

Sun SW, Liang HF, Cross AH, Song SK. Evolving Wallerian degeneration after transient retinal ischemia in mice characterized by diffusion tensor imaging. Neuroimage. 2008; 40:1–10. [PubMed: 18187343]

Sun SW, Liang HF, Schmidt RE, Cross AH, Song SK. Selective vulnerability of cerebral white matter in a murine model of multiple sclerosis detected using diffusion tensor imaging. Neurobiol Dis. 2007; 28:30–38. [PubMed: 17683944]

Trapp BD, Nave KA. Multiple sclerosis: an immune or neurodegenerative disorder? Annu Rev Neurosci. 2008; 31:247–269. [PubMed: 18558855]

Tsurugizawa T, Djemai B, Ciobanu L, Le Bihan D. Diffusion fMRI can detect neural activation when the BOLD fMRI response is abolished by nitroprussiate. Proc Intl Soc Mag Reson Med. 2013; 21:0416.

Tu TW, Budde MD, Quirk JD, Song KS. Using absorption-mode images to improve in vivo DTI quality. Proc Intl Soc Mag Reson Med. 2010; 18:4001.

Tu TW, Wang Y, Chiang CW, Lin TH, Chen YJ, Cross AH, Song SK. Diffusion Basis Spectrum Imaging Detects evolving axonal injury, demyelination and inflammation in the course of EAE. Proc Intl Soc Mag Reson Med. 2012; 20:3598.

van Walderveen MA, Kamphorst W, Scheltens P, van Waesberghe JH, Ravid R, Valk J, Polman CH, Barkhof F. Histopathologic correlate of hypointense lesions on T1-weighted spin-echo MRI in multiple sclerosis. Neurology. 1998; 50:1282–1288. [PubMed: 9595975]

Wang Y, Wang Q, Haldar JP, Yeh FC, Xie M, Sun P, Tu TW, Trinkaus K, Klein RS, Cross AH, Song SK. Quantification of increased cellularity during inflammatory demyelination. Brain. 2011; 134:3590–3601. [PubMed: 22171354]

Waxman SG. Conduction in myelinated, unmyelinated, and demyelinated fibers. Arch Neurol. 1977; 34:585–589. [PubMed: 907529]

Waxman SG. Axonal conduction and injury in multiple sclerosis: the role of sodium channels. Nat Rev Neurosci. 2006; 7:932–941. [PubMed: 17115075]

Wu Q, Butzkueven H, Gresle M, Kirchhoff F, Friedhuber A, Yang Q, Wang H, Fang K, Lei H, Egan GF, Kilpatrick TJ. MR diffusion changes correlate with ultra-structurally defined axonal degeneration in murine optic nerve. Neuroimage. 2007; 37:1138–1147. [PubMed: 17689104]

Zhang CL, Wilson JA, Williams J, Chiu SY. Action potentials induce uniform calcium influx in mammalian myelinated optic nerves. J Neurophysiol. 2006; 96:695–709. [PubMed: 16835363]

Highlights

- Visual stimulation induces a significant $ADC_{\perp}$ decrease in normal mouse optic nerves
- Activation-associated $ADC_{\perp}$ response decreased at the onset of optic neuritis
- Activation-associated $ADC_{\perp}$ response correlated with visual function
- Activation-associated $ADC_{\perp}$ response correlated with optic nerve integrity

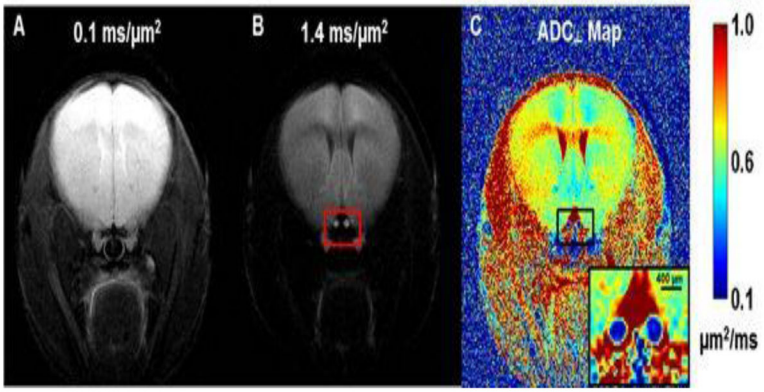

Figure 1.

Two diffusion-weighted images (DWI), which were zero-filled to 512 × 512, with diffusion-sensitizing gradients applied in the phase-encoding direction (left-to-right) with b values of 0.1 ms/μm^2 (or 100 s/mm^2) (A) and 1.4 (B) ms/μm^2 (or 1400 s/mm^2) were used to generate the resulting $ADC_{\perp}$ map (C). The red box in panel B highlights the location of optic nerves (bright) and surrounding cerebrospinal fluid, which is highly suppressed. $ADC_{\perp}$ values in the optic nerves are considerably lower than in other brain tissues. The regular (nearly circular) shape of the optic nerves suggests good orthogonality between the nerve axes and the slice plane, which minimizes partial volume effects.

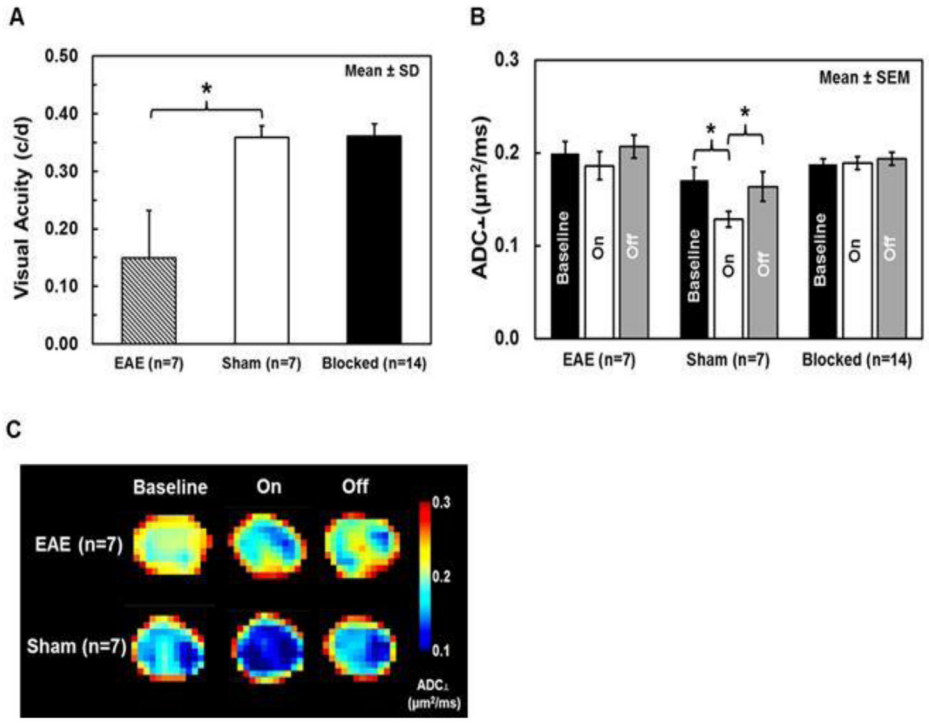

Figure 2.

Group-averaged visual acuity was significantly decreased by 58% ($p < 0.005$, vs. sham) in affected EAE eyes (n=7) compared with the normal vision of sham eyes (n=7); the visual acuity of contralateral blocked (n=14) eyes was in the normal range (A). In this mouse model of EAE optic neuritis, visual deficits typically develop asymmetrically, beginning in only one eye. An activation-associated $ADC_{\perp}$ decrease was observed in both EAE and sham eyes but not in blocked eyes (B, C, and Table 1), suggesting that the decreased $ADC_{\perp}$ in stimulated EAE and sham optic nerves was caused by axonal activity. When compared to its own baseline and stimulus-off, $ADC_{\perp}$ significantly decreased in sham optic nerves by 25 and 22%, respectively (both $p < 0.005$, B, C, and Table 1), with visual stimulation. In contrast, only a slight and non-significant $ADC_{\perp}$ decrease (7%, $p = 0.45$, vs. baseline and 10 %, $p = 0.13$, vs. stimulus-off) was observed in EAE optic nerves (B, C and, Table 1). Group $ADC_{\perp}$ maps of EAE (n=7) and sham (n=7) optic nerves were generated by averaging stacked $ADC_{\perp}$ maps, which were interpolated to 1024 × 1024 (C).

* indicates $p < 0.005$

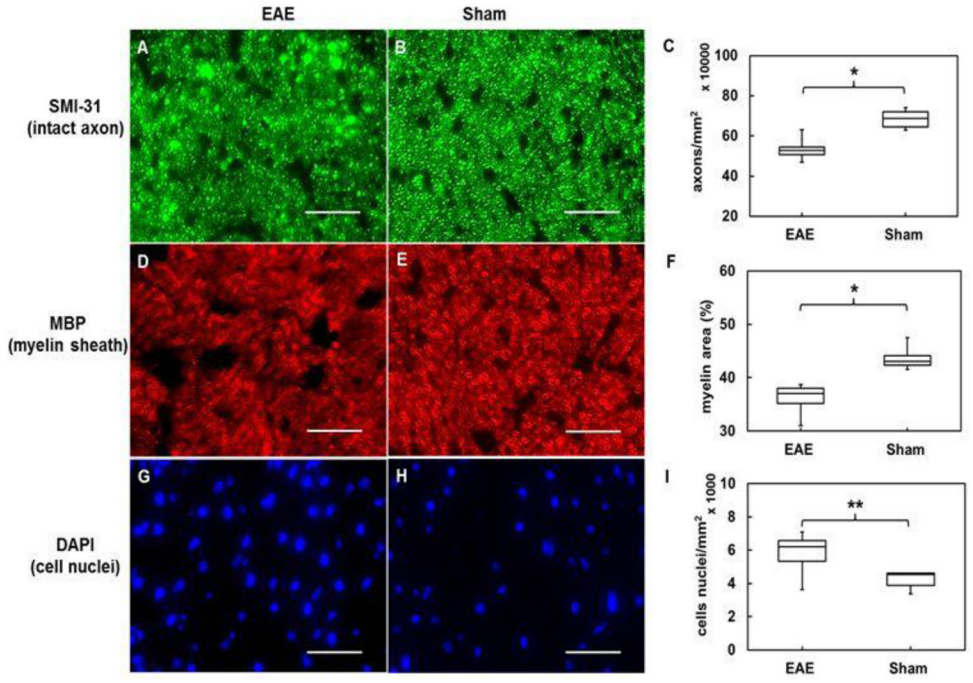

Figure 3.

Representative 60× immunohistochemistry staining images of phosphorylated neurofilaments (SMI-31, intact axons), myelin basic protein (MBP, myelin sheath), and 4′, 6-dianidino-2-phenylindole (DAPI, nuclei) from EAE-affected (A, D, and G,) and sham (B, E, and H) optic nerves. EAE optic nerves with optic neuritis demonstrated obvious axonal beading, lower axonal density (A), reduced myelin area (D), and more cell nuclei (G). Group-averaged IHC counts of EAE (n=7) and sham (n=6) optic nerves (Table 2) revealed significant SMI-31 (C) and MBP (F) decrease ($p < 0.005$) and significant DAPI (I) increase ($p < 0.05$) in the EAE-affected group. IHC results suggested that axonal impairment, demyelination, and inflammatory infiltration all contribute to visual deficits in acute-stage optic neuritis in this EAE mouse model.

Scale Bar: 25 μm

* indicates $p < 0.005$

** indicates $p < 0.05$

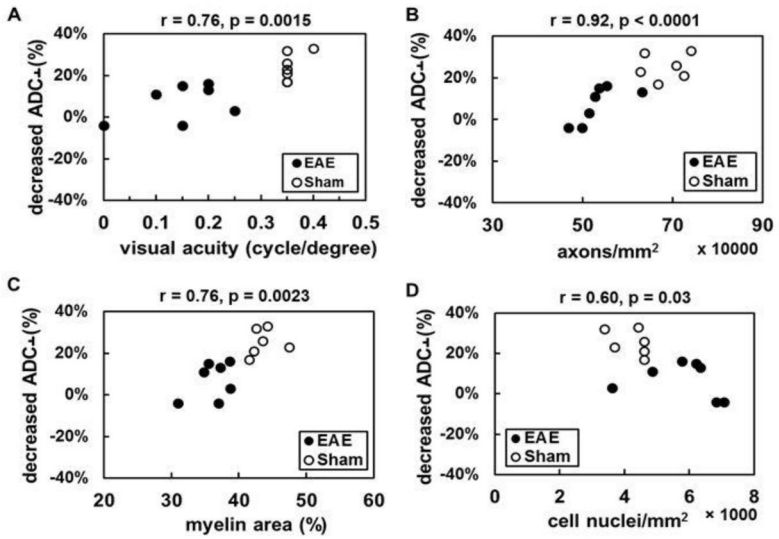

Figure 4.

The activation-associated $ADC_{\perp}$ change (decrease in $ADC_{\perp}$ with stimulation expressed as a percentage of baseline $ADC_{\perp}$) correlated well with visual function (A, r = 0.76, p = 0.0015) and the density of intact axons (B, r = 0.92, p < 0.0001) and myelination (C, r = 0.76, p = 0.0023). Reduced activation-associated $ADC_{\perp}$ response was associated with the severity of inflammation (D, r = 0.60, p = 0.03). These data suggest that axonal impairment and dysfunction can be assessed by diffusion fMRI.

Table 1

Group averaged $ADC_{\perp}$ of baseline, stimulus on, and stimulus off of EAE-affected (n=7), sham (n=7), blocked EAE and sham (n=14) eyes

	Baseline	Stimulus on	Stimulus off
EAE	0.200 ± 0.012	0.186 ± 0.015	0.207 ± 0.012
Sham	0.171 ± 0.014	0.128 ± 0.008	0.164 ± 0.016
Blocked	0.188 ± 0.006	0.189 ± 0.007	0.196 ± 0.007

$ADC_{\perp}$ (μm^2/ms, or $\times 10^{-3}$ mm^2/s): mean ± standard error of the mean

Blocked: contralateral EAE and sham eyes

Table 2

Quantitative immunohistochemistry results of EAE (n=7) and sham (n=6) optic nerves

	SMI31 (#/mm^2)	MBP (area %)	DAPI (#/mm^2)
EAE	5.3 (± 0.6) × 10^5	36.2 ± 2.5	5.8 (± 1.2) × 10^3
Sham	6.8 (± 0.5) × 10^5	43.6 ± 2.1	4.3 (± 0.5) × 10^3

mean ± standard deviation